Extrinsic doping on the atomic scale: Tuning metallicity in atomic Au chains

Z. Mamiyev,[1,2,*] S. Sanna,[3,4] T. Lichtenstein,[1] C. Tegenkamp,[1,2] and H. Pfnür[1,2,†]

[1]*Institut für Festkörperphysik, Leibniz Universität Hannover, Appelstraße 2, 30167 Hannover, Germany*

[2]*Laboratorium für Nano- und Quantenengineering (LNQE), Leibniz Universität Hannover, Schneiderberg 39, 30167 Hannover, Germany*

[3]*Institut für Theoretische Physik, Justus-Liebig-Universität Gießen, Heinrich-Buff-Ring 16, D-35392 Gießen, Germany*

[4]*Center for Materials Research (LaMa), Justus Liebig Universität Gießen, Heinrich-Buff-Ring 16, 35392 Gießen, Germany*

(Received 5 October 2018; revised manuscript received 30 November 2018; published 17 December 2018)

Understanding the response of low-dimensional electronic systems to external perturbations is of great interest for fundamental science as well as future applications. Here we employ plasmon spectroscopy to study the modification of metallicity in Au-induced quantum wires on the Si(553) surface by hydrogenation. The present study shows that no direct bond formation to the Au chains is necessary for controllable modifications of metallicity. Instead, changes in band structure of the whole system by H adsorbed at the Si step edges suffice via indirect interaction, as proven by the quantitative agreement between first-principles calculations and the unoccupied band structure derived from plasmon spectroscopy. Interestingly, simple electron donation has a similar effect as hydrogen adsorption at the step edges with respect to the Au bands and the dimerization of the Au chains.

DOI: 10.1103/PhysRevB.98.245414

I. INTRODUCTION

The reduction of dimension in metallic systems down to quasi-one-dimensional (1D) wires reveals a strikingly rich variability of electronic behavior such as quantization of conductance, extremes of electronic correlation manifested by spin-charge separation, charge and spin density waves [1,2], triplet superconductivity, and Luttinger liquid behavior [3–5]. Due to their inherent instability, however, structural embedding and understanding of the coupling to other dimensions is of high relevance and raises the question of how much of 1D properties survive under experimentally accessible conditions. Depending on step density, step structure, and structural motifs of the metallic chains formed on these surfaces, many 1D properties can still be observed in these quasi-1D systems [6–11].

However, before one can discuss the perspectives of applications of the inherent extreme miniaturization possible with these systems, the extension of basic knowledge in these quantum systems is required. In fact, Au atomic chains on various stepped Si surfaces can serve as versatile and quite variable test objects. Either single or double Au chains are formed on these surfaces, depending on the step orientation. While, e.g., on Si(553) and Si(775) double chains are observed [9,12–15], the (335)- and (557)-oriented Si-Au systems form wires with only a single atomic Au chain on each terrace [12,16].

These surfaces also host plasmonic excitations from mid-infrared to infrared frequency [17,18] with an almost linear dispersion that start at zero energy in the long wavelength limit. In this context, it has been shown only recently that plasmon spectroscopy is a powerful tool to probe these low-lying collective excitations [17,18]. Moreover, the combination of plasmon spectroscopy with quantitative atomistic simulations yields important information about the relation between geometric and electronic structure [18,19], particularly in the unoccupied part close to the Fermi level.

Here we focus on the tunability of metallicity in Au-induced atomic wires on the Si(553) surface by selective chemisorption [19–21], and concentrate on the effect of atomic hydrogen to this surface. The bare surface hosts a double chain of atomic Au wires per terrace after evaporation of 0.48 ML of Au, which generates two surface states that are strongly hybridized with Si [15,22,23]. Only one of them seems to cross the Fermi level and gives rise to quasi-1D metallicity [23]. At the step edge, Si atoms are packed into a graphenelike honeycomb chain with a pair of dangling bonds per sp^2 hybridized Si step edge atom, which shows at low temperature intrinsic magnetic ordering with $\times 3$ periodicity [9]. The latter has also been interpreted as a consequence of a diamagnetic $sp^2 + p$ hybridization [24].

Atomic hydrogen preferentially binds to dangling bonds at Si surfaces [25]. The versatility and tunability of this system was underlined by a most recent study, which combined density functional theory (DFT) calculations with optical reflectance anisotropy (RAS) data [26]. The model calculations of adsorption of atomic hydrogen predict preferential adsorption at the step edge of each terrace (see Fig. 1). As a function of H concentration up to one H atom per Si step edge atom, band filling and modification of bands lead to strong modifications of the band structure to a significant change in Au dimerization. Up to two H atoms per unit cell, now adsorbed on the Si honeycomb chain, were found to be possible. This state is still metallic. These predictions were shown to be compatible with the RAS data.

Since most of the predicted H-induced changes of band structure involve the unoccupied band structure close to the

*mamiyev@fkp.uni-hannover.de

†pfnuer@fkp.uni-hannover.de

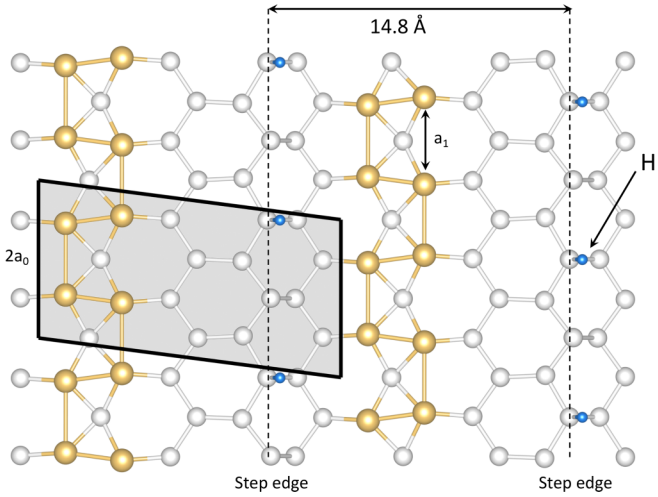

FIG. 1. Top view of the Si(553)-Au surface with atomic hydrogen adsorbed at the Si step edge. Si atoms in white, Au in yellow, and H in blue. The coverage shown corresponds to 1H per (5 × 2) unit cell, which is highlighted in gray. Please note that although the periodic boundary conditions employed in the calculations lead to a regular array of H, adsorbed atoms are most likely not periodically ordered (see below).

Fermi level, which is experimentally very difficult to access, the comparison of theory with experiment is often quite indirect [26]. The purpose of the present study is to get direct access to the H-induced modifications of the band structure above E_F and to compare them again with quantitative DFT. The method used here is momentum-resolved plasmon spectroscopy. Plasmon excitation was shown to be closely related to the upper edge of the electron-hole pair excitations, which in these low-dimensional systems have a quite simple form [27]. If only one band crosses the Fermi level, quantitative predictions of the unoccupied band structure are possible from plasmon spectroscopy, as shown for several examples of quasi-1D systems [19,23].

A. Experimental procedure

Our experiments were performed in an ultrahigh vacuum (UHV) system that hosts a high resolution spot profile analysis low energy electron diffractometer (SPA-LEED) to investigate and control the sample quality, and an electron energy loss spectrometer combined with a SPA-LEED deflection unit (EELS-LEED). This instrument provides high resolution both in energy and in momentum [28]. It has been used to determine plasmon dispersion. The typical operating conditions for these measurements were 12 meV energy resolution and 0.01 $Å^{-1}$ resolution in k space with no mechanical movement of electron source and analyzer. Si(553) samples ($\rho_{Si(553)} \approx 0.01\ \Omega$ cm, n doped) were used for all measurements. After degassing at 600 °C for one day the samples were rapidly annealed at 1250 °C for a few seconds by dc heating with a current flow parallel to the steps, followed by slow cooling to room temperature over several minutes while maintaining the pressure lower than 2×10^{-10} mbar. Au has been evaporated onto a cleaned sample at 630 °C sample temperature at a deposition rate of ∼0.1 ML/min.

A quartz microbalance located at the sample position was used to control the amount of gold with respect to the density of Si atoms in the bulk [111] plane (1 ML = 7.84×10^{14} atoms/cm^2) [28,29]. After preparation the sample was annealed to 950 °C for < 1 s to improve atomic ordering. After this last step a periodic array of nanoscale [111] terraces with a separation of 14.8 Å was observed (see below), which is consistent with previous work [30]. Moreover, after each new preparation a SPA-LEED pattern was taken to check the sample quality. Hydrogen dissociation was induced by a hot filament position in the gas stream at the inlet. The background pressure of H during exposure was typically $\approx2\times10^{-8}$ mbar. After recording reference spectra from the sample without adsorbed H, it was rotated into direct sight of the cracker filament for atomic hydrogen exposure. The flow of atomic hydrogen was estimated as $\sim1\times10^{13}$ $cm^{-2}\,s^{-1}$ assuming a ∼50% cracking efficiency at the hot filament, which, however, covers only a small fraction of the total gas stream of hydrogen. The control experiment with only molecular hydrogen showed no detectable effect even after 100 L hydrogen exposure. After exposure EEL spectra were recorded at constant coverage after the pressure has fallen below 2×10^{-10} mbar. All measurements were carried at room temperature with an integration time of around ∼10 min/scan.

B. Computational details

DFT calculations as implemented in the Vienna *ab initio* simulation package (VASP) [31,32] have been performed within the generalized gradient approximation (GGA) in the Perdew-Burke-Ernzerhof (PBE) formulation [33,34]. Projector augmented waves (PAW) potentials [35,36] with projectors up to $l = 1$ for H, $l = 2$ for Si, and $l = 3$ for Au are used. A number of 1 ($1s^1$), 4 ($3s^2 3p^2$), and 11 ($5d^{10}6s^1$) valence electrons are employed for H, Si, and Au atoms, respectively. Plane waves up to an energy cutoff of 410 eV build up the basis for the electronic wave functions. The silicon surfaces are modeled with asymmetric slabs consisting of six Si bilayers stacked along the [111] crystallographic direction modeling the substrate, the surface termination including the Au chains, and a vacuum region of about 20 Å. Hydrogen atoms saturate the dangling bonds at the lower face of the slabs. These atoms, as well as three Si bilayers, are kept constrained at the experimental lattice constant of 5.4307 Å [37] in order to model the substrate, are free to relax. As suggested by previous investigations [26], only adsorption at the Si step edge is considered. The atomic positions are relaxed until the residual Hellmann-Feynman forces are lower than 0.005 eV/Å. This approach has been found to be suitable for a realistic description of the electronic structure of the Si(553)-Au system [23].

II. RESULTS AND DISCUSSION

A. Band structure calculations

Pure electron donation to the well-defined edge sites, compensated by background charges, was recently found to be sufficient to mimic the influence of H adsorption at the step edges on band structure [26]. Figure 2 shows the effect of additional electronic charge on the Si(553)-Au band structure

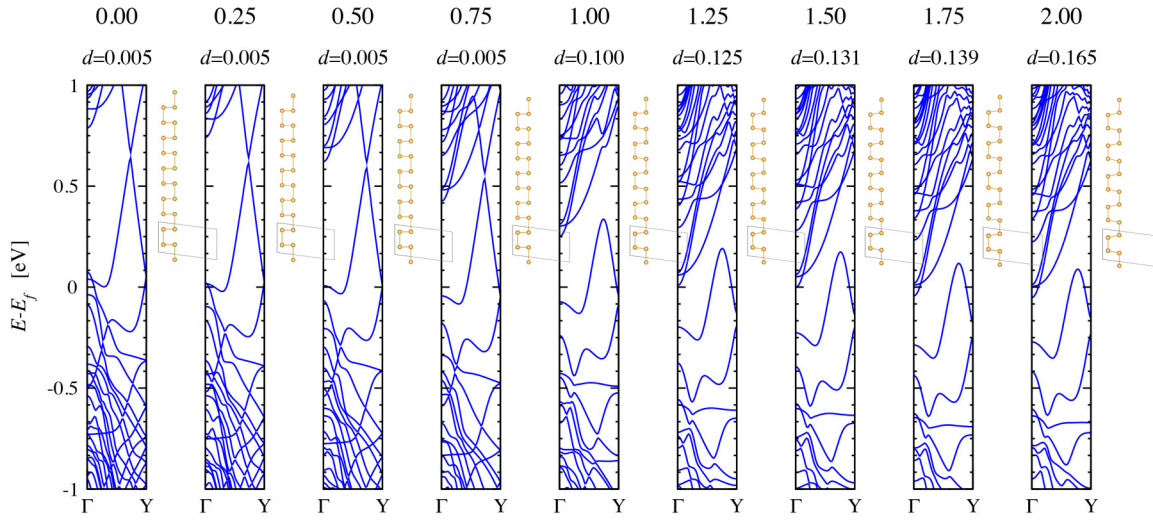

FIG. 2. Electronic band structure of the Si(553)-Au system calculated by DFT as a function of electron doping. The additional elementary charge per (5 × 2) unit cell and the Au dimerization d (see text) are indicated. The Γ-Y direction is roughly parallel to the Au chain.

along the Au chain. The calculations are performed in a (5 × 2) unit cell adding various fractions of an elementary charge. This cell features a full mini-terrace and ×2 periodicity along the chain. It thus allows us to describe the effect of electron doping on the dimerization of the Au chain, too.

At low electron doping concentrations, the band structure modification mainly concerns the occupied states, and leaves bands close to the Fermi level almost unaltered. This situation drastically changes for electron doping higher than 0.75 e per (5 × 2) unit cell. From this point, the Au-derived sp band above E_F starts to shrink and to move downward. The unoccupied bands are rigidly shifted downwards, so that no fundamental band gap can open at any concentration.

The electron doping by addition of external charge is also coupled, but in a highly nonlinear manner, with both the dimerization parameter d defined as the relative deviation of the Au-Au distance from the Si lattice constant a_0, $d = (a_1 - a_0)/a_0$ [9], and with the form of the Au-related bands above the Fermi level. Indeed, only after a certain threshold doping the Au-related bands are occupied, which leads to the observed dimerization enhancement. It has been pointed out recently that artificially increasing the chain dimerization results in an opening of the electronic band gap between the Au related bands [23]. This effect confirms the direct and strong coupling between Au-related electronic bands and chain dimerization.

In conclusion, the calculations shown in Fig. 2 predict an enhancement of the chain dimerization and, in turn, of the ×2 periodicity upon electron doping.

B. Structure from experiment

Adsorption of atomic hydrogen indeed causes enhanced dimerization of the Au chain, as shown directly by the comparison of SPA-LEED patterns from a freshly prepared and from a hydrogenated Si(553)-Au surface, both covered by 0.48 ML of Au (see Fig. 3). The sharp spots in both images, separated by $\Delta k = 0.425\,\text{Å}^{-1}$, indicate a well ordered periodic step structure with (111)-oriented terraces and a terrace width of 14.8 Å, as expected for the (553) orientation for terraces separated by double steps of 3.14 Å height. This pattern qualitatively does not change by H adsorption.

Periodic dimerization of Au atoms along the terraces gives rise to ×2 streaks in the diffraction pattern. These streaks become brighter after exposure to atomic hydrogen, independent of electron energy, and the width of the spot profiles decreases along the [1$\bar{1}$0] direction. These effects indicate an enhanced amplitude of Au dimerization as well as an increase of average length of undistorted dimer chains of Au. On the other hand, H adsorption does not induce any new superstructure so that the H atoms must follow the periodicity of the already existing lattice and must be located at well defined adsorption sites, but there is no long range order of H. H adsorption only causes an increase of background around the central (0×) spots (see spot profile in the right part of Fig. 3).

These findings are compatible with recent theoretical models indicating H adsorption at the Si step edge [26]. They thus legitimate our assumptions for the geometric models adopted to simulate the H adsorption. Furthermore, diffraction exper-

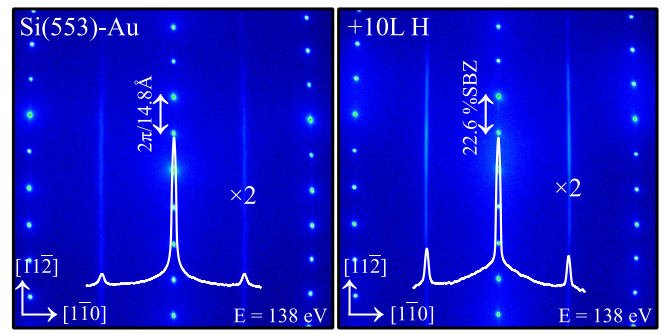

FIG. 3. LEED patterns of Si(553)-Au at a Au concentration of 0.48 ML (left) and the same surface after adsorption of 10 L of atomic hydrogen (right). Line scans (white lines) were generated by integrating the intensities along [11$\bar{2}$] for each k point along the [1$\bar{1}$0] direction and normalization to the central intensity.

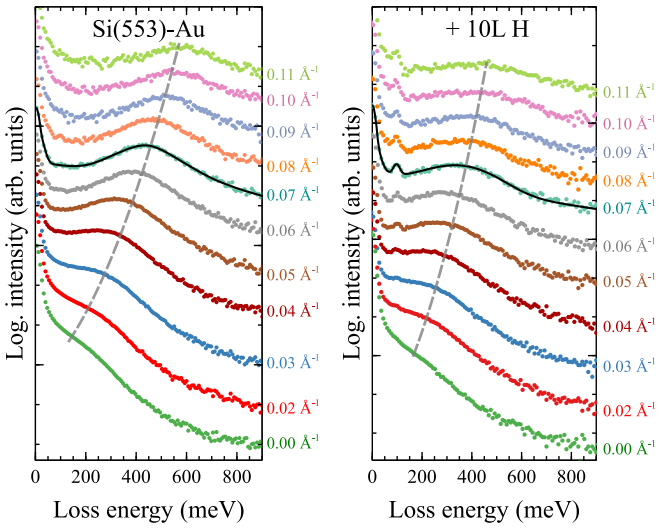

FIG. 4. Momentum-resolved EEL spectra taken along the [1$\bar{1}$0] direction for Si(553)-Au (a) and after exposure to 10 L of atomic hydrogen (b). The dashed lines indicate the plasmon losses dispersing only in $k_\parallel$ along the terraces. An exemplary fit is depicted as an overlay in both data sets at $k_\parallel = 0.07$ Å^{-1}. Spectra were shifted versus each other for better visibility.

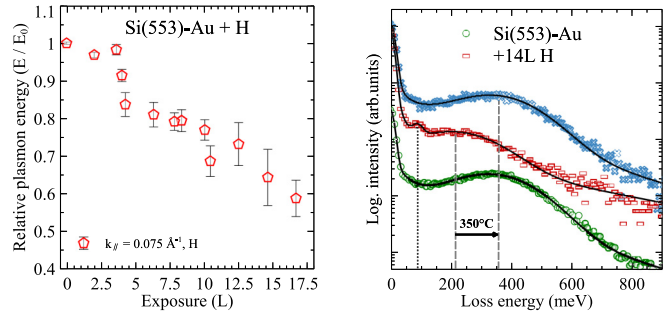

FIG. 5. Left: Reduction of plasmon frequency, exemplified for $k_\parallel = 0.075$ Å, as a function of hydrogen exposure. Please note that only about 1% of this exposure is atomic H. Right: Reversibility of H-induced shifts of plasmonic losses in Si(553)-Au. $k_\parallel = 0.05$ Å^{-1}. Green: EEL spectrum without H, red: after hydrogen adsorption. Blue: after thermal desorption of H at 350 °C. Spectra were shifted against each other.

iments corroborate the theoretical findings of a H-induced enhancement of Au dimerization.

C. Plasmonic excitations

In order to obtain more insight into the electron excitation spectrum, we recorded momentum-resolved EEL spectra. Dispersing losses (measurements at room temperature) were only found in the direction along the terraces. Only this direction is shown in Fig. 4. The comparison between clean and hydrogenated Si(553)-Au reveals broad loss features that are attributed to the plasmonic excitation [38]. In addition, a small sharp and nondispersing loss peak close to 100 meV was found that we assigned to the Si-H bending vibrational mode [39], which seems to be shifted upward with respect to the Si(111) surface. We excluded any electron beam induced effects by continuous exposure of the hydrogenated surface to the electron beam over 7 h and found no changes compared with the freshly prepared surface.

Qualitatively, the anisotropic plasmonic excitation is not altered upon hydrogen adsorption. However, the plasmon dispersion is reduced gradually by hydrogen exposure, as illustrated in Fig. 4. The increase of hydrogen exposure is coupled with a reduction of loss intensity (see Figs. 4 and 5) so that it becomes nondetectable after ∼15 L of H exposure. This behavior indicates that adsorbed H atoms are not ordered. On the contrary, the H-induced disorder is a plausible reason for the reduction of loss intensity with increasing H exposure. Furthermore, the exponential decay of loss intensity as a function of loss energy, described as Drude tail [40], indicates that metallicity is preserved under all conditions measured here.

As a function of exposure, a significant reduction of plasmon frequency was observed only for exposures above 3.5 L, whereas changes were negligible at smaller exposures. The dependence of plasmon frequency on exposure is shown exemplarily at a fixed $k_\parallel$ of 0.075 Å^{-1} in the left part of Fig. 5. This finding is in good qualitative agreement with the behavior predicted by the simulations shown in Fig. 2. If only a single type of sites at the step edges is occupied, as assumed in the model calculations, this finding implies a strong concentration dependent reduction also of the sticking probability. This property would partly compensate, but not remove the nonlinear response of plasmon excitation to H doping found in the simulations.

The H-induced redshift of the plasmon loss turned out to be reversible upon heating of the sample to 350 °C (see right part of Fig. 5), which leads to desorption of the hydrogen.

Plasmon dispersions as a function of $k_\parallel$ have been extracted from the peak positions of plasmonic losses by applying the same fit routine to all spectra [41]. These are shown for clean and hydrogenated surfaces in Fig. 6. The H-induced reduction of slope in the dispersion is now seen more clearly. While minor changes are already seen at an H exposure of 4 L, the slope is about 30% smaller at 10 L. Comparing with the calculations of Sec. II A, the excitation spectrum from E_F to empty states above E_F is virtually unchanged up to an average occupation probability of the Si step edge of about 0.35. This number must be exceeded with the 4 L exposure, while only a relatively small increment up to less than 0.5 is necessary to explain the observed changes of slope in dispersion.

Furthermore, it is obvious from Fig. 6 that the data after H exposure deviate from the extrapolation to zero energy in the long wavelength limit. This finding is compatible with the assumption of H-induced disorder that reduces the possibility of free propagation of plasmonic waves to the limit where only dispersionless standing waves still can exist. Such standing waves make excitation of plasmons by infrared radiation (IR) possible, which actually has been observed in this system [20].

For a quantitative analysis of the plasmon dispersion, we make use of the close relationship between the upper edge of the electron-hole continuum and the plasmon dispersion, which for quasi-1D systems turns out to be particularly simple [18]. If the quasi-1D array of wires is considered as a 2D electron gas that is confined to a wire of finite width by an

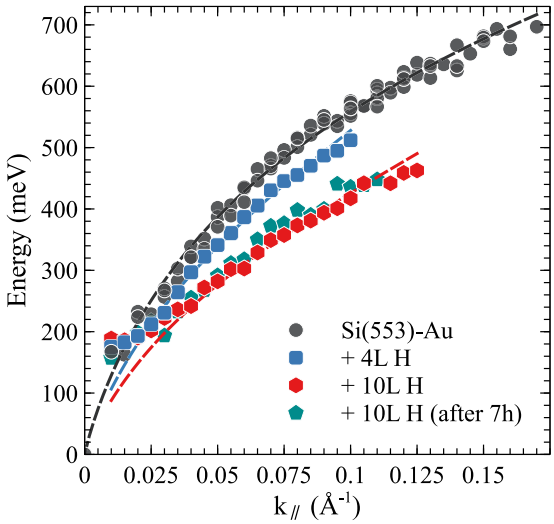

FIG. 6. Plasmon dispersion curves before and after adsorption of various amounts of atomic H, as determined from the respective loss peak positions. The solid lines are guides to the eye, only assuming that the dispersion curves have to start at zero in the long wavelength limit.

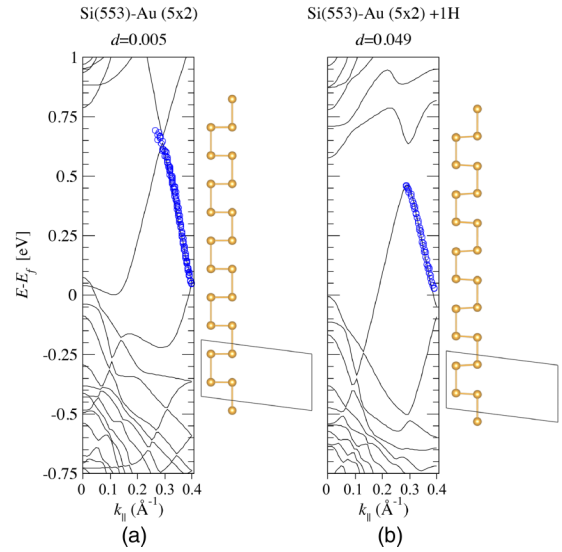

FIG. 7. Calculated electronic band structures for the clean and the hydrogenated surfaces. The dimerization of the clean and after H adsorption is shown schematically at the right side of the respective band structure. The upper boundary of single particle excitations, derived from the plasmon dispersion by the procedure described in the text, is marked by blue circles for the clean (a) and the hydrogenated surface (b).

appropriate potential [27], the plasmon dispersion for a single isolated wire can be expressed as a function of the upper and lower boundary of the electron-hole continuum of excitations ω_+ and ω_-, respectively. Here we take the relationship derived in Ref. [27] and solve it for ω_+, which then reads

$$\omega_+(k_\parallel) = \sqrt{\frac{\omega_p^2(k_\parallel)(e^{A(k_\parallel)} - 1) + \omega_-^2(k_\parallel)}{e^{A(k_\parallel)}}}, \qquad (1)$$

with

$$A(k) = \frac{\hbar^2 2\pi k}{m^\star g_s V(k)[1 - G(k)]}.$$

$V(k)$ is the Fourier transform of the confining potential, $G(k)$ is the local field correction factor due to electronic correlations, and g_s is the spin degeneracy (1 or 2). For ω_p the experimentally determined plasmon dispersions were used. ω_- was obtained from the calculated band structure, shown in Fig. 2 with the assumption that the topmost occupied Au-induced band can be approximated by a parabola close to E_F. For the determination of the dispersion of ω_+, ω_- has only a significant influence very close to Fermi energy. Therefore, if there is only one unoccupied band above E_F, as in all cases investigated here, ω_+ should coincide closely with this band. ω_+ determined from the measured plasmon dispersion and from ω_-, as just described, is shown in Fig. 7 for the clean (a) as well as for the hydrogenated surface [after 10 L H exposure (b)] together with the calculated band structures.

This even quantitative agreement of the dispersion of ω_+ with the calculated band structure, as derived from plasmon spectroscopy after adsorption of 10 L of H, is remarkable and again proves the usefulness of plasmon spectroscopy for getting quantitative information about the unoccupied part of the band structure close to the Fermi level. Furthermore, it gives clear evidence for H-induced widening of the band gap to about 0.2 eV. This widening is coupled with an increase of the amplitude of dimerization by roughly one order of magnitude. This increase is in nice agreement with the enhanced intensity of the ×2 streaks in LEED, since this amplitude should be directly proportional to the integrated diffracted intensity (note the log scale in Fig. 3).

The band structure of the Si(553)-Au system without hydrogen and the significance of plasmon spectroscopy for clarification of structural details like the amplitude of dimerization of the Au chains was also the subject of a recent investigation [23]. As shown there, dimerization and band gap opening in the vicinity of $E = 0.7$ eV above E_F are linearly related, starting from a very small value for the clean system.

Our results are also in qualitative agreement with the calculations by Hogan *et al.*, and corroborate the interconnection between band gap opening and dimerization [26]. This interrelation is caused by the hybridization of Au-related bands with the Si surface bands near to the Fermi level [23]. The modification of the unoccupied band structure due to this hybridization and its significant deviation from a parabolic dispersion prevents the plasmon dispersion to enter the electron-hole pair continuum (or Landau damping zone). In other words, the free-electron gas picture turns out not to be adequate for the description of plasmon dispersion in this class of systems.

The disorder introduced by hydrogen adsorption in this system affects strongly its plasmonic properties and limits the range of observability in k space. For this reason, the metal-insulator transition predicted from simulations at the DFT-LDA level of accuracy [26] is experimentally not accessible. Further theoretical and experimental investigation are necessary to further investigate this topic.

III. CONCLUSIONS

This combined study of low energy electron diffraction, plasmon spectroscopy, and calculations with density functional theory provides evidence for an adsorbate induced doping mechanism exclusively of surface states. While metallicity turns out to be strongly coupled with the Au-induced surface bands, adsorption of atomic hydrogen has a direct influence on these bands, although the preferential adsorption site is at the Si step edge, which is not in direct contact with the Au double chain. In other words, each mini-terrace should be considered as an entity and the assignment of bands to structural subgroups, e.g., the Au chains, is questionable.

Hydrogen acts as a low-dimensional donor shifting surface bands down with respect to the Fermi level. However, as seen from our simulations, due to concomitant changes of the band structure, the resulting changes, e.g., of plasmon frequency, are highly nonlinear as a function of H concentration: No changes of plasmon frequencies are seen up to almost one additional electron per (5×2) unit cell. Interestingly, while local relaxations at the adsorption sites of H play a marginal role in this context, band filling is coupled directly with the dimerization of the Au atoms [23], i.e., band filling and metallicity can be tuned by changes in Au dimerization and vice versa. This mechanism only works because H adsorption at the Si step edge takes place in a random manner so that it does not destroy the $\times 2$ periodicity of the Au chain.

Since the partially filled band crossing the Fermi level is more than half-filled, a further increase of the Fermi level reduces the plasmon dispersion. From simulation results [26] it seems, however, that complete passivation of the surface by atomic hydrogen will not destroy the electrical conductance. This is important for any application in which the structure has to be passivated and embedded into nonconductive material. We have not tested the robustness of this type of passivation with only moderate chemisorption strength, which, as shown, can be reversibly desorbed at $\sim$350 °C.

From a more fundamental point of view, the present study provides crucial insight into the tunability of metallicity in subnanometric wires on semiconductor surfaces. In particular, we demonstrate an indirect but effective approach for fine tuning of the dimerization and conductivity of the wires by modifications of substrate regions that are not in close proximity of the chains. This opens up the possibility of further turning knobs affecting directly and indirectly the wire geometry. Modifications of the substrate lattice constant (e.g., via Si_xGe_{1-x} alloys) or of its free carrier concentration (e.g., by n-type volume doping of the substrate) are examples of the first and of the second, respectively. This tuning is essential for fundamental quantum physics as well, as it brings such systems closer to the use in nanoelectronics. The unexpected effect of doping on metallicity also opens fundamental questions about the diversity of adsorbate-surface interactions.

ACKNOWLEDGMENTS

We gratefully acknowledge financial support from the DFG in the research unit FOR 1700 (projects E4 and T1) and Niedersächsisches Ministerium für Wissenschaft und Kultur through the graduate school "contacts in nanosystems." The Höchstleistungrechenzentrum Stuttgart (HLRS) is gratefully acknowledged for grants of high-performance computer time. We acknowledge computational resources provided by the HPC Core Facility and the HRZ of the Justus-Liebig-Universität Gießen.

[1] S. Kagoshima, H. Nagasawa, and T. Sambongi, *One-Dimensional Conductors*, Springer Series in Solid-State Sciences Vol. 72 (Springer, Berlin, 1988), pp. 126–135.
[2] G. Grüner, Rev. Mod. Phys. **60**, 1129 (1988).
[3] J. M. Luttinger, J. Math. Phys. **4**, 1154 (1963).
[4] K. Schönhammer, in *Strong Interactions in Low Dimensions*, Physics and Chemistry of Materials with Low-Dimensional Structures, edited by L. D. D. Baeriswyl (Springer Netherlands, Dordrecht, 2004), Vol. 25, Chap. 4, pp. 93–136.
[5] T. Giamarchi, *Quantum Physics in One Dimension* (Clarendon, Oxford, 2007).
[6] C. Zeng, P. Kent, T.-H. Kim, A.-P. Li, and H. H. Weitering, Nat. Mater. **7**, 539 (2008).
[7] P. C. Snijders and H. H. Weitering, Rev. Mod. Phys. **82**, 307 (2010).
[8] H. Weitering, Nat. Phys. **7**, 744 (2011).
[9] S. C. Erwin and F. J. Himpsel, Nat. Commun. **1**, 58 (2010).
[10] J. Aulbach, J. Schäfer, S. C. Erwin, S. Meyer, C. Loho, J. Settelein, and R. Claessen, Phys. Rev. Lett. **111**, 137203 (2013).
[11] C. Brand, H. Pfnür, G. Landolt, S. Muff, J. H. Dil, T. Das, and C. Tegenkamp, Nat. Commun. **6**, 8118 (2015).
[12] J. N. Crain, J. L. McChesney, F. Zheng, M. C. Gallagher, P. C. Snijders, M. Bissen, C. Gundelach, S. C. Erwin, and F. J. Himpsel, Phys. Rev. B **69**, 125401 (2004).
[13] I. Barke, F. Zheng, T. K. Rügheimer, and F. J. Himpsel, Phys. Rev. Lett. **97**, 226405 (2006).
[14] J. Aulbach, S. C. Erwin, R. Claessen, and J. Schäfer, Nano Lett. **16**, 2698 (2016).
[15] M. Krawiec, Phys. Rev. B **81**, 115436 (2010).
[16] M. Krawiec and M. Jałochowski, Phys. Rev. B **87**, 075445 (2013).
[17] T. Nagao, S. Yaginuma, T. Inaoka, and T. Sakurai, Phys. Rev. Lett. **97**, 116802 (2006).
[18] T. Lichtenstein, Z. Mamiyev, C. Braun, S. Sanna, W. G. Schmidt, C. Tegenkamp, and H. Pfnür, Phys. Rev. B **97**, 165421 (2018).
[19] Z. Mamiyev, T. Lichtenstein, C. Tegenkamp, C. Braun, W. G. Schmidt, S. Sanna, and H. Pfnür, Phys. Rev. Mater. **2**, 066002 (2018).
[20] F. Hötzel, Ph.D. thesis, Ruprecht-Karls-Universität Heidelberg, 2017.
[21] S. Suchkova, C. Hogan, F. Bechstedt, E. Speiser, and N. Esser, Phys. Rev. B **97**, 045417 (2018).

[22] I. Song, D.-H. Oh, H.-C. Shin, S.-J. Ahn, Y. Moon, S.-H. Woo, H. J. Choi, C.-Y. Park, and J. R. Ahn, Nano Lett. **15**, 281 (2015).
[23] S. Sanna, T. Lichtenstein, Z. Mamiyev, C. Tegenkamp, and H. Pfnür, J. Phys. Chem. C **122**, 25580 (2018).
[24] C. Braun, U. Gerstmann, and W. G. Schmidt, Phys. Rev. B **98**, 121402 (2018).
[25] C. Beitia, W. Preyss, R. Del Sole, and Y. Borensztein, Phys. Rev. B **56**, R4371(R) (1997).
[26] C. Hogan, E. Speiser, S. Chandola, S. Suchkova, J. Aulbach, J. Schäfer, S. Meyer, R. Claessen, and N. Esser, Phys. Rev. Lett. **120**, 166801 (2018).
[27] R. K. Moudgil, V. Garg, and K. N. Pathak, J. Phys.: Condens. Matter **22**, 135003 (2010).
[28] H. Claus, A. Büssenschütt, and M. Henzler, Rev. Sci. Instrum. **63**, 2195 (1992).
[29] G. Sauerbrey, Z. Phys. **155**, 206 (1959).
[30] P. C. Snijders, S. Rogge, and H. H. Weitering, Phys. Rev. Lett. **96**, 076801 (2006).
[31] G. Kresse and J. Furthmüller, Comput. Mater. Sci. **6**, 15 (1996).
[32] G. Kresse and J. Furthmüller, Phys. Rev. B **54**, 11169 (1996).
[33] J. P. Perdew, J. A. Chevary, S. H. Vosko, K. A. Jackson, M. R. Pederson, D. J. Singh, and C. Fiolhais, Phys. Rev. B **46**, 6671 (1992).
[34] J. P. Perdew, K. Burke, and M. Ernzerhof, Phys. Rev. Lett. **77**, 3865 (1996).
[35] G. Kresse and D. Joubert, Phys. Rev. B **59**, 1758 (1999).
[36] P. E. Blöchl, Phys. Rev. B **50**, 17953 (1994).
[37] R. W. G. Wyckoff, *Crystal Structures* (Interscience, New York, 1963), Vol. 1.
[38] T. Lichtenstein, J. Aulbach, J. Schäfer, R. Claessen, C. Tegenkamp, and H. Pfnür, Phys. Rev. B **93**, 161408 (2016).
[39] H. Kobayashi, K. Edamoto, M. Onchi, and M. Nishijima, J. Chem. Phys. **78**, 7429 (1983).
[40] B. N. J. Persson and J. E. Demuth, Phys. Rev. B **30**, 5968 (1984).
[41] U. Krieg, T. Lichtenstein, C. Brand, C. Tegenkamp, and H. Pfnür, New J. Phys. **17**, 043062 (2015).